

HIGH-PERFORMANCE COMPUTING FOR THE BGK MODEL OF THE BOLTZMANN EQUATION WITH A MESHFREE ARBITRARY LAGRANGIAN-EULERIAN METHOD

PANCHATCHRAM MARIAPPAN*, KLAAS WILLEMS †, GANGADHARA BOREGOWDA*,
SUDARSHAN TIWARI † AND AXEL KLAR †

Abstract. In this paper, we present high-performance computing for the BGK model of the Boltzmann equation with a mesh-free method. For the numerical simulation of the BGK equation we use an Arbitrary-Lagrangian-Eulerian (ALE) method developed in previous work, where the approximation of spatial derivatives and the reconstruction of a function is based on the weighted least squares method. A Graphics Processing Unit (GPU) is used to accelerate the code. The result is compared with sequential and parallel versions of the CPU code. Two and three-dimensional driven cavity problems are solved, where a speed-up of several orders of magnitude is obtained compared to a sequential CPU simulation.

Keywords. rarefied gas, kinetic equation, BGK model, meshfree method, ALE method, least squares, GPU computing

AMS Classification. 65M99, 74P05, 70E99

1. Introduction. During the last two decades simulation of Micro Electro Mechanical Systems (MEMS) has attracted many researchers, see [19, 24, 8, 31, 26, 25, 2, 35, 36]. This is mostly micro-nano fluidics, where the mean free path is often of the order or larger than the characteristic length of the geometry. That means, the Knudsen number, i.e. the ratio of the mean free path and the characteristic length, is of the order 1 or larger. In this case, one has to solve rarefied gas flows modelled by the Boltzmann equation. Usually, these flows have low Mach numbers, therefore, stochastic methods like Direct Simulation Monte Carlo (DSMC) [3] are not the optimal choice, since statistical noise dominates the flow quantities. Moreover, when one considers moving a rigid body, the gas domain changes in time and one encounters unsteady flow problems such that averages over long runs cannot be taken. Instead, one has to perform many independent runs and average the solutions to obtain the smooth solutions, which is time consuming. Although some attempts have been made to reduce the statistical noise of DSMC-type methods, see, for example, [9], or to adopt efficient solvers for the Boltzmann equation, such as those based on the Fourier-spectral method (see for example the review paper [11]), many works rather employ deterministic approaches for simplified models of the Boltzmann equation, like the Bhatnagar-Gross-Krook (BGK) model, see [24, 8, 35, 32, 33].

This paper is based on an earlier paper [34] describing a mesh-free Arbitrary Lagrangian-Eulerian (ALE) method for the BGK equation. There, we have solved two-dimensional problems with moving objects inside a rarefied flow. The computational costs for such simulations are high due to the high dimensionality of the problem. This is particularly true for 3D problems where in addition to the three space dimensions, a further 3 velocity dimensions have to be considered for the BGK equations. Thus, reasonably accurate numerical simulations require a suitable parallelization procedure. In the present paper, such a procedure using Graphics Processing Unit (GPU) computations is presented and numerically investigated.

*Department of Mathematics, RPTU Kaiserslautern-Landau, Erwin-Schrödinger-Straße, 67663 Kaiserslautern, Germany ({klar, tiwari}@mathematik.uni-kl.de, klaas.willems@math.rptu.de)

†Department of Mathematics and Statistics, Indian Institute of Technology Tirupati, India (ma19d502, panch.m@iittp.ac.in)

In this paper, we exploit the GPU which is well-known for massively parallel computing. Researchers have developed and demonstrated the advantage of GPUs for kinetic models using various schemes such as DSMC [13, 14, 15], the Lattice Boltzmann method [7, 6, 29, 21, 1], discrete unified gas kinetic scheme [22], direct numerical simulation [39] and a semi-Lagrangian approach [10].

The paper is organized as follows. In section 2, we present the BGK model for the Boltzmann equation including the Chu reduction procedure used for 2D computations. In section 3, we present the numerical scheme for the BGK model, in particular the spatial and temporal discretization using a first-order discretization method. In section 4, we present the GPU architecture and the implementation of the numerical scheme in GPU. In section 5, we present numerical results in two and three-space dimensions. Finally, in section 6 some conclusions and an outlook are presented.

2. The BGK model for rarefied gas dynamics. We consider the BGK model of the Boltzmann equation for rarefied gas dynamics, where the collision term is modeled by a relaxation of the distribution function $f(t, \mathbf{x}, \mathbf{v})$ to the Maxwellian equilibrium distribution. The evolution equation for the distribution function $f(t, \mathbf{x}, \mathbf{v})$ is given by the following initial boundary value problem

$$\frac{\partial f}{\partial t} + \mathbf{v} \cdot \nabla_{\mathbf{x}} f = \frac{1}{\tau}(M - f), \quad (2.1)$$

with $f(0, \mathbf{x}, \mathbf{v}) = f_0(\mathbf{x}, \mathbf{v})$, $t \geq 0$, $\mathbf{x} \in \Omega \subset \mathbb{R}^{d_x}$, ($d_x = 1, 2, 3$), $\mathbf{v} \in \mathbb{R}^{d_v}$, ($d_v = 1, 2, 3$) and suitable initial and boundary conditions described in the next section. Here τ is the relaxation time and M is the local Maxwellian given by

$$M = \frac{\rho}{(2\pi RT)^{d_v/2}} \exp\left(-\frac{|\mathbf{v} - \mathbf{U}|^2}{2RT}\right), \quad (2.2)$$

where the parameters $\rho(t, \mathbf{x}) \in \mathbb{R}$, $\mathbf{U}(t, \mathbf{x}) \in \mathbb{R}^{d_v}$, $T(t, \mathbf{x}) \in \mathbb{R}$ are the macroscopic quantities density, mean velocity and temperature, respectively. R is the universal gas constant. ρ, \mathbf{U}, T are computed from f as follows. Let the moments of f be defined by

$$(\rho, \rho\mathbf{U}, E) = \int_{\mathbb{R}^3} \phi(\mathbf{v}) f(t, \mathbf{x}, \mathbf{v}) d\mathbf{v}. \quad (2.3)$$

where $\phi(\mathbf{v}) = \left(1, \mathbf{v}, \frac{|\mathbf{v}|^2}{2}\right)$ denotes the vector of collision invariants. E is the total energy density which is related to the temperature through the internal energy

$$e(t, x) = \frac{3}{2}RT, \quad \rho e = E - \frac{1}{2}\rho|\mathbf{U}|^2. \quad (2.4)$$

The relaxation time $\tau = \tau(x, t)$ and the mean free path λ are related according to [4]

$$\tau = \frac{4\lambda}{\pi\bar{C}}, \quad (2.5)$$

where $\bar{C} = \sqrt{\frac{8RT}{\pi}}$ and the mean free path is given by

$$\lambda = \frac{k_b}{\sqrt{2}\pi\rho R d^2}, \quad (2.6)$$

where k_b is the Boltzmann constant and d is the diameter of the gas molecules.

2.1. Chu-reduction. To solve two dimensional flow problems with $d_x = 2$ one might consider mathematically a two-dimensional velocity space $d_v = 2$ since the consideration of three-dimensional velocity space requires unnecessary high memory and computational time. However, it is physically correct to consider in these situations still three dimensional velocity space. In these cases, for the BGK model, the 3D velocity space can be reduced as suggested by Chu [5]. This reduction yields a considerable reduction in memory allocations and computational time. For example, in a physically two-dimensional situation, in which all variables depend on $\mathbf{x} \in \mathbb{R}^2$ and t , the velocity space is reduced from three dimensions to two dimensions defining the following reduced distributions [17]. Considering $\mathbf{v} = (v_1, v_2, v_3) \in \mathbb{R}^3$ we define

$$g_1(t, x, v_1, v_2) = \int_{\mathbb{R}} f(t, x, v_1, v_2, v_3) dv_3 \quad (2.7)$$

$$g_2(t, x, v_1, v_2) = \int_{\mathbb{R}} v_3^2 f(t, x, v_1, v_2, v_3) dv_3. \quad (2.8)$$

Multiplying (2.1) by 1 and v_3^2 and integrating with respect to $v_3 \in \mathbb{R}$, we obtain the following system of two equations denoting for simplicity $(v_1, v_2) = \mathbf{v}$ in the reduced equations.

$$\frac{\partial g_1}{\partial t} + \mathbf{v} \cdot \nabla_{\mathbf{x}} g_1 = \frac{1}{\tau} (G_1 - g_1) \quad (2.9)$$

$$\frac{\partial g_2}{\partial t} + \mathbf{v} \cdot \nabla_{\mathbf{x}} g_2 = \frac{1}{\tau} (G_2 - g_2), \quad (2.10)$$

where

$$G_1 = \int_{\mathbb{R}} M dv_3 = \frac{\rho}{2RT} \exp\left(\frac{|\mathbf{v} - \mathbf{U}|^2}{2RT}\right) \quad (2.11)$$

$$G_2 = \int_{\mathbb{R}} v_3^2 M dv_3 = (RT)G_1 \quad (2.12)$$

with $\mathbf{U} = (U_1, U_2) \in \mathbb{R}^2$. Assuming that it is a local equilibrium, the initial distributions are defined via the parameters $\rho_0, \mathbf{U}_0, T_0$ and are given as

$$g_1(0, \mathbf{x}, \mathbf{v}) = \frac{\rho_0}{2RT_0} \exp\left(\frac{|\mathbf{v} - \mathbf{U}_0|^2}{2RT_0}\right), \quad g_2(0, \mathbf{x}, \mathbf{v}) = (RT_0)g_1(0, \mathbf{x}, \mathbf{v}). \quad (2.13)$$

The macroscopic quantities are given through the reduced distributions as

$$\rho = \int_{\mathbb{R}^2} g_1 d\mathbf{v}, \quad \rho \mathbf{U} = \int_{\mathbb{R}^2} \mathbf{v} g_1 d\mathbf{v}, \quad 3\rho RT = \int_{\mathbb{R}^2} |v - U|^2 g_1 d\mathbf{v} + \int_{\mathbb{R}^2} g_2 d\mathbf{v}. \quad (2.14)$$

3. Numerical schemes. We solve the original equation (2.1) in three-dimensional physical space and the reduced system of equations (2.9 - 2.10) in two-dimensional physical space by the ALE method described below. We use a time splitting, where the advection step is solved explicitly and the relaxation part is solved implicitly, and a meshfree particle method to solve this system of equations while approximating the spatial derivatives. Here, by particle, we actually mean grid points moving with the mean velocity \mathbf{U} of the gas. The spatial derivatives of the distribution function at an arbitrary particle position are approximated using values at the point cloud surrounding the particle and a weighted least squares method.

3.1. ALE formulation. One of the most widely used deterministic methods for the BGK equation is the semi-Lagrangian method. The semi-Lagrangian method is based on fixed grids. For flows with moving boundaries, meshfree methods with moving grids might be more suitable than fixed grids, see [33, 34]. For such a method one rewrites the equations as follows.

3.1.1. ALE formulation for original model. We rewrite the equations (2.1) in Lagrangian form as

$$\frac{d\mathbf{x}}{dt} = \mathbf{U} \quad (3.1)$$

$$\frac{df}{dt} = -(\mathbf{v} - \mathbf{U}) \cdot \nabla_{\mathbf{x}} f + \frac{1}{\tau}(M - f) \quad (3.2)$$

where $\frac{d}{dt} = \frac{\partial}{\partial t} + \mathbf{U} \cdot \nabla_{\mathbf{x}}$. The first equation describes motion with the macroscopic mean velocity \mathbf{U} of the gas determined by (2.14). The second equation includes the remaining advection with the difference between microscopic and macroscopic velocity.

3.1.2. ALE for reduced model. In this case the equations (2.7 - 2.8) are reformulated in Lagrangian form as

$$\frac{d\mathbf{x}}{dt} = \mathbf{U} \quad (3.3)$$

$$\frac{dg_1}{dt} = -(\mathbf{v} - \mathbf{U}) \cdot \nabla_{\mathbf{x}} g_1 + \frac{1}{\tau}(G_1 - g_1) \quad (3.4)$$

$$\frac{dg_2}{dt} = -(\mathbf{v} - \mathbf{U}) \cdot \nabla_{\mathbf{x}} g_2 + \frac{1}{\tau}(G_2 - g_2). \quad (3.5)$$

3.2. Time discretization. The above equations are discretized with the following scheme.

3.2.1. First order time splitting scheme for original model. Time is discretized as $t^n = n\Delta t, n = 0, 1, \dots, N_t$. We denote the numerical approximation of f at t_n by $f^n = f(t^n, \mathbf{x}, \mathbf{v})$. We use a time splitting scheme for equation (3.2), where the advection term is solved explicitly and the collision term is solved implicitly. In the first step of the splitting scheme we obtain the intermediate distribution \tilde{f}^n by solving

$$\tilde{f}^n = f^n - \Delta t(\mathbf{v} - \mathbf{U}^n) \cdot \nabla_{\mathbf{x}} f^n. \quad (3.6)$$

In the second step, we obtain the new distribution by solving

$$f^{n+1} = \tilde{f}^n + \frac{\Delta t}{\tau}(M^{n+1} - \tilde{f}^n) \quad (3.7)$$

and the new positions of the grids are updated by

$$\mathbf{x}^{n+1} = \mathbf{x}^n + \Delta t \mathbf{U}^{n+1}. \quad (3.8)$$

In the first step, we have to approximate the spatial derivatives of f at every grid point. This is described in the following section.

Following [16, 17, 37] we obtain f^{n+1} in the second step by first determining the parameters $\rho^{n+1}, \mathbf{U}^{n+1}$ and T^{n+1} for M^{n+1} . Multiplying (3.7) by 1, \mathbf{v} and $|\mathbf{v} - \mathbf{U}|^2$ and integrating over velocity space, we get

$$\rho^{n+1} = \int_{\mathbb{R}^3} \tilde{f}^n d\mathbf{v}, \quad (\rho \mathbf{U})^{n+1} = \int_{\mathbb{R}^3} \mathbf{v} \tilde{f}^n d\mathbf{v}, \quad 3\rho RT^{n+1} = \int_{\mathbb{R}^3} |\mathbf{v} - \mathbf{U}|^2 \tilde{f}^n d\mathbf{v}, \quad (3.9)$$

where we have used the conservation of mass, momentum and energy of the original BGK model.

Now, the parameters ρ^{n+1} , \mathbf{U}^{n+1} and T^{n+1} of M^{n+1} are given in terms of \tilde{f} from (3.9) since ρ, U and T of f and M are same. Hence the implicit step (3.7) can be rewritten as

$$f^{n+1} = \frac{\tau \tilde{f}^n + \Delta t M^{n+1}}{\tau + \Delta t}. \quad (3.10)$$

3.2.2. Time splitting scheme for the reduced model. We use again a time splitting scheme. In the first step we obtain the intermediate distributions \tilde{g}_1^n and \tilde{g}_2^n by solving for $\mathbf{v} \in \mathbb{R}^2$ and $\mathbf{U} \in \mathbb{R}^2$

$$\tilde{g}_1^n = g_1^n - \Delta t (\mathbf{v} - \mathbf{U}^n) \cdot \nabla_{\mathbf{x}} g_1^n \quad (3.11)$$

$$\tilde{g}_2^n = g_2^n - \Delta t (\mathbf{v} - \mathbf{U}^n) \cdot \nabla_{\mathbf{x}} g_2^n. \quad (3.12)$$

In the second step, we obtain the new distributions by solving

$$g_1^{n+1} = \tilde{g}_1^n + \frac{\Delta t}{\tau} (G_1^{n+1} - g_1^{n+1}) \quad (3.13)$$

$$g_2^{n+1} = \tilde{g}_2^n + \frac{\Delta t}{\tau} (G_2^{n+1} - g_2^{n+1}) \quad (3.14)$$

and the new positions of the grids are updated by

$$\mathbf{x}^{n+1} = \mathbf{x}^n + \Delta t \mathbf{U}^{n+1}. \quad (3.15)$$

For the second step, we have to determine first the parameters ρ^{n+1} , U^{n+1} and T^{n+1} for G_1^{n+1} and G_2^{n+1} . Multiplying (3.13) by 1 and v and integrating with respect to v over \mathbb{R}^2 we get

$$\rho^{n+1} = \int_{\mathbb{R}^2} \tilde{g}_1^n d\mathbf{v}, \quad (\rho U)^{n+1} = \int_{\mathbb{R}^2} v \tilde{g}_1^n d\mathbf{v}, \quad (3.16)$$

where we have used the conservation of mass and momentum of the original BGK model. In order to compute T^{n+1} we note that the following identity is valid

$$\int_{\mathbb{R}^2} |\mathbf{v} - \mathbf{U}|^2 (G_1 - g_1) d\mathbf{v} + \int_{\mathbb{R}^2} (G_2 - g_2) d\mathbf{v} = 0. \quad (3.17)$$

Multiplying the equation (3.13) by $|\mathbf{v} - \mathbf{U}|^2$ and integrate with respect to \mathbf{v} over \mathbb{R}^2 we get

$$\int_{\mathbb{R}^2} |\mathbf{v} - \mathbf{U}|^2 g_1^{n+1} d\mathbf{v} = \int_{\mathbb{R}^2} |\mathbf{v} - \mathbf{U}|^2 \tilde{g}_1^n d\mathbf{v} + \frac{\Delta t}{\tau} \int_{\mathbb{R}^2} |\mathbf{v} - \mathbf{U}|^2 (G_1^{n+1} - g_1^{n+1}) d\mathbf{v}. \quad (3.18)$$

Next, integrate both sides of (3.14) with respect to \mathbf{v} over \mathbb{R}^2 we get

$$\int_{\mathbb{R}^2} g_2^{n+1} d\mathbf{v} = \int_{\mathbb{R}^2} \tilde{g}_2^n d\mathbf{v} + \frac{\Delta t}{\tau} \int_{\mathbb{R}^2} (G_2^{n+1} - g_2^{n+1}) d\mathbf{v}. \quad (3.19)$$

Adding (3.18) and (3.19) and making use of the identity (3.17) we get

$$3\rho^{n+1} R T^{n+1} = \int_{\mathbb{R}^2} |\mathbf{v} - \mathbf{U}|^2 \tilde{g}_1^n d\mathbf{v} + \int_{\mathbb{R}^2} \tilde{g}_2^n d\mathbf{v}. \quad (3.20)$$

Now, the parameters ρ^{n+1} , \mathbf{U}^{n+1} and T^{n+1} of G_1^{n+1} and G_2^{n+1} are given in terms of \tilde{g}_1^n and \tilde{g}_2^n from (3.16) and (3.20). Hence the implicit steps (3.13) and (3.14) can be rewritten as

$$g_1^{n+1} = \frac{\tau \tilde{g}_1^n + \Delta t G_1^{n+1}}{\tau + \Delta t} \quad (3.21)$$

$$g_2^{n+1} = \frac{\tau \tilde{g}_2^n + \Delta t G_2^{n+1}}{\tau + \Delta t}. \quad (3.22)$$

3.3. Velocity discretization. We consider N_v velocity grid points and a uniform velocity grid of size $\Delta v = 2v_{\max}/N_v$. We assume that the distribution function is negligible for $|v| > v_{\max}$ and discretize $[-v_{\max}, v_{\max}] \times [-v_{\max}, v_{\max}] \times [-v_{\max}, v_{\max}]$. That means for each velocity direction we have the discretization points $v_j = -v_{\max} + (j-1)\Delta v$, $j = 1, \dots, N_v + 1$. Note that the performance of the method could be improved by using a grid adapted to the mean velocity \mathbf{U} , see, for example, [8].

3.4. Spatial discretization. We discuss the spatial discretization and upwinding procedures for first-order schemes.

3.4.1. Approximation of spatial derivatives. In the above numerical schemes, an approximation of the spatial derivatives of f or g_1 and g_2 is required. In this subsection, we describe a least squares approximation of the derivatives on the moving point cloud based on so-called generalized finite differences, see [28] and references therein. A stabilizing procedure using upwinding discretization will be described in the following.

We consider a three-dimensional spatial domain $\Omega \cup \Gamma \in \mathbb{R}^3$, where Γ is the boundary. We first approximate the boundary of the domain by a set of discrete points called boundary particles. In the second step, we approximate the interior of the computational domain using another set of interior points or interior particles. The sum of boundary and interior points gives the total number of points. We note that the boundary conditions are applied on the boundary points. If the boundary moves, the boundary points also move together with the boundary. The initial generation of grid points can be regular as well as arbitrary. When the points move they can form a cluster or can scatter away from each other. In these cases, either some grid points have to be removed or new grid points have to be added. We will describe this particle management in a forthcoming subsection.

Let $f(\mathbf{x})$ be a scalar function and f_i its discrete values at $\mathbf{x}_i = (x_i, y_i, z_i)$. We consider the problem of approximating the spatial derivatives of a function f at \mathbf{x}_i from the values of its neighboring points. In principle, all points can be neighbors, however, we associate a weight function such that nearby particles have higher and far away particles have lesser influence such that we obtain an accurate approximation of derivatives. So, one can choose a weight as a function of the distance between the central point and its neighbor. The distance function decays as the distance goes to infinity. In this paper, we have considered a Gaussian function, but other choices are possible (see for example [27, 38] for other classes of weight functions). In order to limit the number of neighboring points we consider only the neighbors inside a circle of radius h with center \mathbf{x}_i . We choose as radius h some factor of the average spacing Δx , such that we have at least a minimum number of neighbors for the least-squares approximation, even next to the boundary. In the case of regular grid far from the boundary, one might consider using smaller values of h . Such adaptive choice of h has been considered, for example, in [20]. For the sake of simplicity, we have chosen

a constant $h = 3.1 \Delta x$ in this paper, which gives a sufficiently large number of neighbours. Let $P(\mathbf{x}_i; h) = \{\mathbf{x}_{i_j}, j = 1, \dots, m(h)\}$ denote the set of neighbor points of \mathbf{x}_i inside the disc of radius h . We note that the number m of neighbours depends on h . In all calculations, we have considered the following truncated Gaussian weight function

$$w(\|\mathbf{x}_{i_j} - \mathbf{x}_i\|; h) = \begin{cases} \exp(-\alpha \frac{\|\mathbf{x}_{i_j} - \mathbf{x}_i\|^2}{h^2}), & \text{if } \frac{\|\mathbf{x}_{i_j} - \mathbf{x}_i\|}{h} \leq 1 \\ 0, & \text{else,} \end{cases}$$

with α a user-defined positive constant, chosen here as $\alpha = 6$, so that the influence of far neighbor grid points is negligible. This choice is based on previous experiences [20, 30].

We consider the m Taylor expansions of $f(x_{i_j}, y_{i_j}, z_{i_j})$ around (x_i, y_i, z_i)

$$f_{i_j} = f(x_{i_j}, y_{i_j}, z_{i_j}) = f_i + \frac{\partial f}{\partial x}(x_{i_j} - x_i) + \frac{\partial f}{\partial y}(y_{i_j} - y_i) + \frac{\partial f}{\partial z}(z_{i_j} - z_i) + e_{i_j}, \quad (3.23)$$

for $j = 1, \dots, m$, where e_{i_j} is the error in the Taylor's expansion. We note that the discrete values f_{i_j} are known. The system of equations (3.23) can be re-expressed as

$$\begin{aligned} f_{i_1} - f_i &= \frac{\partial f}{\partial x}(x_{i_1} - x_i) + \frac{\partial f}{\partial y}(y_{i_1} - y_i) + \frac{\partial f}{\partial z}(z_{i_1} - z_i) + e_{i_1} \\ &\vdots \\ &\vdots \\ f_{i_m} - f_i &= \frac{\partial f}{\partial x}(x_{i_m} - x_i) + \frac{\partial f}{\partial y}(y_{i_m} - y_i) + \frac{\partial f}{\partial z}(z_{i_m} - z_i) + e_{i_m}. \end{aligned} \quad (3.24)$$

The system of equations can be written in matrix form as

$$\mathbf{e} = \mathbf{b} - M\mathbf{a}, \quad (3.25)$$

where $\mathbf{e} = [e_{i_1}, \dots, e_{i_m}]^T$, $\mathbf{a} = [\frac{\partial f}{\partial x}, \frac{\partial f}{\partial y}, \frac{\partial f}{\partial z}]^T$, $\mathbf{b} = [f_{i_1} - f_i, \dots, f_{i_m} - f_i]^T$ and

$$M = \begin{pmatrix} x_{i_1} - x_i & y_{i_1} - y_i & z_{i_1} - z_i \\ \vdots & \vdots & \vdots \\ x_{i_m} - x_i & y_{i_m} - y_i & z_{i_m} - z_i \end{pmatrix}.$$

If the number of neighbors m is larger than three, this system of equations is over-determined for three unknowns $\mathbf{a} = [\frac{\partial f}{\partial x}, \frac{\partial f}{\partial y}, \frac{\partial f}{\partial z}]^T$. The unknowns \mathbf{a} are obtained from the weighted least squares method by minimizing the quadratic form

$$J = \sum_{j=1}^m w_j e_j^2 = (M\mathbf{a} - \mathbf{b})^T W (M\mathbf{a} - \mathbf{b}), \quad (3.26)$$

where $W = w_j \delta_{jk}$, $k = 1, \dots, m$ is the diagonal matrix. The minimization of J yields

$$\mathbf{a} = (M^T W M)^{-1} (M^T W) \mathbf{b}. \quad (3.27)$$

Denoting $S = (S_{ij}) = (M^T W M)^{-1}$ as the 3×3 symmetric matrix and denoting $dx_j = x_{i_j} - x_i$, $dy_j = y_{i_j} - y_i$, $dz_j = z_{i_j} - z_i$ the vector $(M^T W) \mathbf{b}$ is explicitly given by

$$(M^T W) \mathbf{b} = \begin{pmatrix} \sum_{j=1}^m w_j dx_j (f_{i_j} - f_i) \\ \sum_{j=1}^m w_j dy_j (f_{i_j} - f_i) \\ \sum_{j=1}^m w_j dz_j (f_{i_j} - f_i) \end{pmatrix}. \quad (3.28)$$

Equating the first component of vectors of (3.27) we obtain the approximation of the spatial derivatives

$$\frac{\partial f}{\partial x} = \sum_{j=1}^m w_j (S_{11} dx_j + S_{12} dy_j + S_{13} dz_j) (f_{i_j} - f_i) \quad (3.29)$$

$$\frac{\partial f}{\partial y} = \sum_{j=1}^m w_j (S_{21} dx_j + S_{22} dy_j + S_{23} dz_j) (f_{i_j} - f_i) \quad (3.30)$$

$$\frac{\partial f}{\partial z} = \sum_{j=1}^m w_j (S_{31} dx_j + S_{32} dy_j + S_{33} dz_j) (f_{i_j} - f_i). \quad (3.31)$$

The corresponding computations are done for the two-dimensional case. We note that higher-order approximations are obtained by using higher-order Taylor's expansion in (3.23). We refer to [30] for details.

In the above least-squares approximation, a function is approximated at an arbitrary point from its neighboring points and the distribution of these points can be arbitrary. Such a straightforward least-squares approximation leads to a central difference scheme. In case of discontinuities in the solution, this will lead to numerical oscillations and one has to introduce additional numerical viscosity. This can be done in the least squares framework by a suitable upwind reconstruction described in the next subsection.

3.4.2. First order upwind scheme. First, we describe the procedure for two-dimensional physical space. The naive method for computing upwind derivatives is to only use neighbor particles in the 'upwind'-half of the plane from the central particle. For example, we compute the x-partial derivatives of f in the following way. If $v_1 - U_1 > 0$, we sort the neighbors with $x_{i_j} \leq x_i$ and then compute the derivatives considering Taylor's expansion (3.23) and then using the least squares method. Similarly, if $v_1 - U_1 < 0$ we use the set of neighbors with $x_{i_j} \geq x_i$. For y-derivatives we use the upper half and lower half of the neighbors according to the sign of $v_2 - U_2$. In a two-dimensional case, we have to use four stencils and in a three-dimensional case, we have to use 6 stencils, which is time-consuming. Moreover, the positivity of the scheme is not guaranteed. Therefore, we have used a positive scheme suggested in [23].

The scheme suggested in [23] makes use of one single central stencil and is, thus, computationally more efficient than the approach described above. Moreover, due to the additional diffusion that is added, the scheme is positive. In the following, we describe shortly the positive upwind scheme reported in [23].

Two dimensional physical space: In the explicit step of 3.6 we have to compute the flux, for example, at the discrete point x_i

$$\mathbf{Q}(f)_i = (v_1 - U_1) \frac{\partial f}{\partial x} + (v_2 - U_2) \frac{\partial f}{\partial y}. \quad (3.32)$$

Using (3.29 - 3.30) we can re-express (3.32) as

$$\mathbf{Q}(f)_i = (v_1 - U_1) \sum_{j=1}^m \alpha_{ij} (f_{i_j} - f_i) + (v_2 - U_2) \sum_{j=1}^m \alpha_{ij} (f_{i_j} - f_i), \quad (3.33)$$

where

$$\begin{aligned}\alpha_{ij} &= w_j(S_{11} dx_j + S_{12} dy_j) \\ \beta_{ij} &= w_j(S_{21} dx_j + S_{22} dy_j)\end{aligned}$$

Let $\phi_{ij} = \text{atan2}(\frac{dy_i}{dx_j})$ be the angle between positive x-axis and the line $x_i x_{i_j}$ joining two points x_i and x_{i_j} . Let $\mathbf{n}_{ij} = (\cos \phi_{ij}, \sin \phi_{ij})$ be the unit vector along $x_i x_{i_j}$. Let $\mathbf{t}_{ij} = (-\sin \phi_{ij}, \cos \phi_{ij})$ be the unit vector orthogonal to \mathbf{n}_{ij} so that $((\mathbf{n}_{ij}, \mathbf{t}_{ij}))$ form a right handed coordinate system. Then the convective vector $\mathbf{v} - \mathbf{U}$ can be written in terms of this coordinate system after a rotational transformation

$$\begin{aligned}v_1 - U_1 &= ((\mathbf{v} - \mathbf{U}) \cdot \mathbf{n}_{ij} \cos \phi_{ij} - ((\mathbf{v} - \mathbf{U}) \cdot \mathbf{t}_{ij}) \sin \phi_{ij} \\ v_2 - U_2 &= ((\mathbf{v} - \mathbf{U}) \cdot \mathbf{n}_{ij} \sin \phi_{ij} + ((\mathbf{v} - \mathbf{U}) \cdot \mathbf{t}_{ij}) \cos \phi_{ij}.\end{aligned}$$

Then after using mid-point flux approximations along \mathbf{n}_{ij} and \mathbf{t}_{ij} together with the upwind approximation of the flux the upwind approximation of (3.32) is obtained in the form

$$\begin{aligned}\mathbf{Q}(f)_i &= \sum_{j=1}^m \bar{\alpha}_{ij} [(\mathbf{v} - \mathbf{U}) \cdot \mathbf{n}_{ij} - |(\mathbf{v} - \mathbf{U}) \cdot \mathbf{n}_{ij}|] (f_{i_j} - f_i) + \\ &\sum_{j=1}^m \bar{\beta}_{ij} [(\mathbf{v} - \mathbf{U}) \cdot \mathbf{t}_{ij} - \text{sign}(\bar{\beta}_{ij}|(\mathbf{v} - \mathbf{U}) \cdot \mathbf{t}_{ij}|)] (f_{i_j} - f_i),\end{aligned}\quad (3.34)$$

where

$$\begin{aligned}\bar{\alpha}_{ij} &= \alpha_{ij} \cos \phi_{ij} + \beta_{ij} \sin \phi_{ij} \\ \bar{\beta}_{ij} &= -\alpha_{ij} \sin \phi_{ij} + \beta_{ij} \cos \phi_{ij}.\end{aligned}$$

Three dimensional physical space: As in the two dimensional case, the velocity is re-expressed in terms of the component along $x_i x_{i_j}$ and the two normal directions. We define these vectors as

$$A = \begin{pmatrix} n_{ij}(1) & n_{ij}(2) & n_{ij}(3) \\ t_{ij}(1) & t_{ij}(2) & t_{ij}(3) \\ b_{ij}(1) & b_{ij}(2) & b_{ij}(3) \end{pmatrix} = \begin{pmatrix} \sin \theta_{ij} \cos \phi_{ij} & \sin \theta_{ij} \sin \phi_{ij} & \cos \theta_{ij} \\ \cos \theta_{ij} \cos \phi_{ij} & \cos \theta_{ij} \sin \phi_{ij} & -\sin \theta_{ij} \\ -\sin \phi_{ij} & \cos \phi_{ij} & 0 \end{pmatrix}.$$

where $\phi_{ij} = \text{atan2}(\frac{dy_j}{dx_j})$, $\theta_{ij} = \arccos(\frac{dz_j}{r})$, $r = \sqrt{dx_j^2 + dy_j^2 + dz_j^2}$.

Now using (3.29 - 3.31) we can re-express (3.32) as

$$\mathbf{Q}(f)_i = (v_1 - U_1) \sum_{j=1}^m \alpha_{ij} (f_{i_j} - f_i) + (v_2 - U_2) \sum_{j=1}^m \alpha_{ij} (f_{i_j} - f_i) + (v_3 - U_3) \sum_{j=1}^m \gamma_{ij} (f_{i_j} - f_i),$$

where

$$\begin{aligned}\alpha_{ij} &= w_j(S_{11} dx_j + S_{12} dy_j + S_{13} dz_j) \\ \beta_{ij} &= w_j(S_{21} dx_j + S_{22} dy_j + S_{23} dz_j) \\ \gamma_{ij} &= w_j(S_{31} dx_j + S_{32} dy_j + S_{33} dz_j)\end{aligned}$$

Writing the convective velocity vector $v - U$ in terms of coordinate systems (n_{ij}, t_{ij}, b_{ij}) with

$$\begin{pmatrix} v_1 - U_1 \\ v_2 - U_2 \\ v_3 - U_3 \end{pmatrix} = A^t \begin{pmatrix} \langle \mathbf{v} - \mathbf{U}, \mathbf{n}_{ij} \rangle \\ \langle \mathbf{v} - \mathbf{U}, \mathbf{t}_{ij} \rangle \\ \langle \mathbf{v} - \mathbf{U}, \mathbf{b}_{ij} \rangle \end{pmatrix}$$

and the rotational coefficients $\bar{\alpha}_{ij}, \bar{\beta}_{ij}, \bar{\gamma}_{ij}$ as

$$\begin{pmatrix} \bar{\alpha}_{ij} \\ \bar{\beta}_{ij} \\ \bar{\gamma}_{ij} \end{pmatrix} = A^t \begin{pmatrix} \alpha_{ij} \\ \beta_{ij} \\ \gamma_{ij} \end{pmatrix}$$

we have the upwind approximation of flux and is given as

$$\begin{aligned} \mathbf{Q}(f)_i &= \sum_{j=1}^m \bar{\alpha}_{ij} [(\mathbf{v} - \mathbf{U}) \cdot \mathbf{n}_{ij} - |(\mathbf{v} - \mathbf{U}) \cdot \mathbf{n}_{ij}|] (f_{i_j} - f_i) + \\ &\sum_{j=1}^m \bar{\beta}_{ij} [(\mathbf{v} - \mathbf{U}) \cdot \mathbf{t}_{ij} - \text{sign}(\bar{\beta}_{ij}|(\mathbf{v} - \mathbf{U}) \cdot \mathbf{t}_{ij}|)] (f_{i_j} - f_i) + \\ &\sum_{j=1}^m \bar{\gamma}_{ij} [(\mathbf{v} - \mathbf{U}) \cdot \mathbf{t}_{ij} - \text{sign}(\bar{\gamma}_{ij}|(\mathbf{v} - \mathbf{U}) \cdot \mathbf{b}_{ij}|)] (f_{i_j} - f_i) \end{aligned} \quad (3.35)$$

3.5. Particle management. In this section we discuss shortly some technical aspects of meshfree methods like, for example, neighbour searching, adding as well as removing particles, see [20, 12, 34] for more details.

3.5.1. Neighbour search. Searching neighbouring grid points at an arbitrary position is the most important and most time-consuming part of the meshfree method. Since the positions of grid points change at time, we have to search neighbor lists at every time step. We refer to [34] for details.

3.5.2. Adding and removing points. When grid points move in time, they either scatter or cluster. When they scatter, there may be holes in the computational domain and there are not enough neighbors at these point, such that the numerical scheme becomes unstable. Therefore, one has to add new particles. On the other hand if grid points cluster, there might be unnecessarily large numbers of neighbors at certain points, which requires more computational time and, moreover, leads to a strongly non-uniform distribution of points causing bad condition number. In this case, if two points are close to each other, we remove both of them and introduce a new grid in the mid-point. Then we update the distribution function $f(t, \mathbf{x}, \mathbf{v})$ on these new grid points with the help of the least squares method. We refer to [32] for a more detailed discussions.

4. GPU Architecture and CUDA Implementation. Modern GPUs, developed by NVIDIA and AMD have thousands of smaller efficient cores that can run multiple tasks simultaneously. However, typical bottlenecks of GPUs are data transfer between CPUs and GPUs, low levels of memory, and power consumption. Further, not all computational tasks can be parallelized efficiently to utilize the GPU architecture.

4.1. CPU and GPU Architecture. In this work, the serial version of the code is implemented in g++ version 9.4.0 with `-Ofast` optimization and Eigen [18] on an Intel(R) Xeon(R) Gold 6126 @ 2.40GHz, 768 GB RAM system under Rocky Linux 8.10. The OpenMP (OMP) parallel version of the code is implemented in g++ version 9.4.0 with `-fopenmp` flag and Eigen on the same CPU architecture with 80 threads. The GPU simulations are performed on an Intel(R) Xeon(R) Gold 6126 @ 2.40GHz, 768 GB RAM system with an NVIDIA Tesla A100 (80 GB Memory, 6912 CUDA cores at 1.41 GHz GPU max clock rate with 3 copy engines). The CUDA code is implemented on CUDA v12.4.1 with `-O3` and `-use_fast_math`.

4.2. CUDA Implementation. Particles are initialized with a `struct` variable that carries information about the position (x, y, z) , velocity (U, V, W) , density ρ , temperature T , neighbouring voxel, neighbors, number of neighbours, distributions $\tilde{g}_1, \tilde{g}_2, g_1, g_2, \tilde{f}, f$. The size of each particle is at least 31KB in the case of a two-dimensional problem and 157KB for a three-dimensional case for $N_v = 20$. Hence, for example, for the two-dimensional case with 250000 particles the CUDA implementation uses at least 7GB. In the current setting, 10000, 40000, 90000, 160000 and 250000 particles are generated for the two-dimensional case and 8000, 27000 and 64000 particles are generated for the three-dimensional case to observe the efficiency of the GPU and CPU code.

All particles are generated using the CUDA version and particle memory is allocated using `cudaMallocManaged` to avoid the memory transfer between CPU and GPU. With the help of this managed memory, particle information is accessible by both the CPU and GPU. The following algorithm is implemented in CUDA for three-dimensional velocity.

1. CUDA allocates the required managed memory for each particle.
2. Generate all particles and index them from 0 to $N - 1$. Each CUDA thread generates a particle.
3. Divide the domain into voxels, index it from 0 to $\text{vox} - 1$, identify the neighbour voxel for each voxel and store it in the voxel database, each CUDA thread updates this information.
4. For each particle, identify its respective voxel index using each CUDA thread.
5. Loop over time
 - (a) Neighbor Search: For each particle, iterate through its voxel and neighbouring voxel and identify the list of neighbor indices using each CUDA thread.
 - (b) Particle Organization: Add or remove particles.
 - (c) Loop over $N_v + 1 \times N_v + 1 \times N_v + 1$
 - i. Initial Conditions: Apply the initial conditions on each particle using the CUDA thread
 - ii. Spatial Derivatives: Approximate the spatial derivatives and apply the upwind scheme for each particle where each CUDA thread computes least-square approximation and applies the upwind scheme.
 - iii. Moments: Compute the moments for each particle using each thread.
 - iv. Boundary Conditions: Apply boundary conditions for each boundary particle using each thread.

5. Numerical results. As numerical test-cases we consider kinetic driven cavity problems in 2D and 3D.

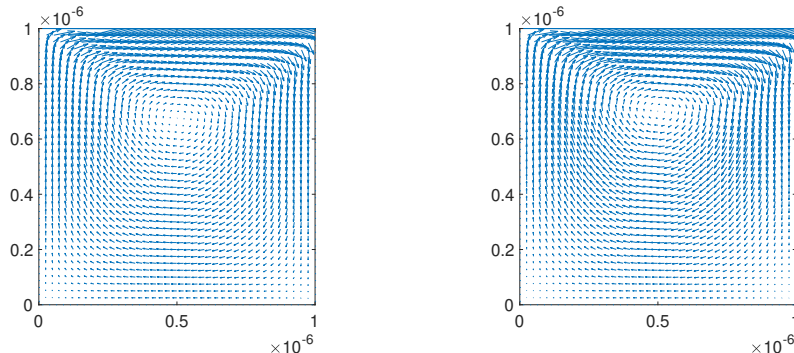


Fig. 5.1: Two dimensional driven cavity velocity vectors for Knudsen numbers and Reynolds numbers $Kn = 1.1, Re = 2.968 \times 10^{-4}$ (left) and $Kn = 0.11, Re = 2.968 \times 10^{-5}$ (right).

5.1. Two dimensional driven cavity problem. In this case, we use the two-dimensional BGK model that makes use of the Chu-reduction (see 3.2.2). We consider a square cavity $[0, L] \times [0, L]$ with $L = 1 \times 10^{-6}$. Here L is considered as the characteristic length. We consider Argon gas with diameter $d = 0.368 \times 10^{-9}$, the Boltzmann constant $k_B = 1.3806 \times 10^{-23}$ and the gas constant $R = 208$. Initially the gas is in thermal equilibrium and the distribution function is the Maxwellian distribution with initial parameters $\mathbf{U}_0 = 0, T_0 = 270$. We consider densities $\rho_0 = 1$ and 0.1 such that their corresponding Knudsen numbers are $Kn = 1.1$ and $Kn = 0.11$, respectively. From Eq. 2.5 the corresponding relaxation times are $\tau = 3.7142 \times 10^{-10}$ and $\tau = 3.7142 \times 10^{-9}$. We apply diffuse reflection boundary conditions on all walls, where we keep constant temperature $T_{wall} = T_0$ and the wall velocity \mathbf{U}_{wall} . The top wall has the velocity $\mathbf{U}_{wall} = (1, 0)$ and other walls have zero velocities. The number of velocity grid points is $N_v = 20$. The spatial grid points are initially generated in a regular way with numbers ranging from 100 to 500 for each spatial direction. When they move, their distribution will become random after few time steps. We have chosen a constant time step $\Delta t = 1 \times 10^{-11}$ for all resolutions.

In Fig. 5.1 we have plotted the velocity vectors in steady state for both Knudsen numbers. We note that Mach and Reynolds number are very small for these computations. We have performed the same simulation on both the CPU and the GPU. In Table 5.1 we present the GPU computation time and speedup compared to serial and parallel CPU computation times. We have used the above mentioned range of resolution in physical space and a fixed velocity grid with $N_v = 20$. We also report the memory required to store the grid. As expected, we observe that the GPU speed up is higher compared to both serial and parallel CPUs, when finer resolutions are used. For 200×200 grid points, we obtain a speedup of about 29 times with a single thread and 4 times with 80 threads on the CPU, where as for a 500×500 grid, the GPU speedup is about 307 times for the single thread CPU and 47 times for the multithreaded (80 threads) CPU.

5.2. Three dimensional driven cavity problem. In this case we consider a cube $[0, L] \times [0, L] \times [0, L]$ with $L = 1 \times 10^{-6}$. Initially, the grid consists of N regular grid points. As already mentioned, the regular distribution of grid points is destroyed after some time steps. The initial parameters of the Maxwellian are the same as in

$N \times N_v^3$	Time (min)			Speedup		Memory
	CPU	OMP	GPU	CPU vs GPU	OMP vs GPU	
$200^2 \times 20^2$	87	13	3	29	4	1.6GB
$300^2 \times 20^2$	626	53	6	104	9	3.7GB
$400^2 \times 20^2$	2314	200	10	231	20	5.5GB
$500^2 \times 20^2$	3640	587	12.5	307	47	7.5GB

Table 5.1: GPU Speedup for 2D Driven Cavity.

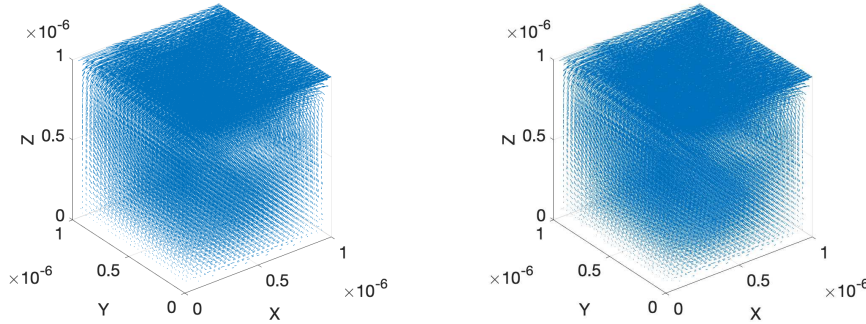


Fig. 5.2: Three dimensional driven cavity velocity vectors for Knudsen numbers and Reynolds numbers $Kn = 1.1, Re = 2.968 \times 10^{-4}$ (left) and $Kn = 0.11, Re = 2.968 \times 10^{-5}$ (right).

the previous 2d case. We use again diffuse reflection boundary conditions with fixed temperature T_0 on all boundaries. On the top wall $z = L$, we prescribe a non-zero velocity in x -direction given by

$$\mathbf{U} = (1, 0, 0).$$

On other five walls, all velocities are zero. In Fig. 5.2 we have plotted the velocity vectors for about 30000 particles for Knudsen numbers $Kn = 1.1$ and 0.11 . Moreover, in Fig. 5.3 we have plotted the velocity vectors in xz plane at $y = 0.5 \times 10^{-6}$ for both Knudsen numbers. One observes that the results are qualitatively the same for both Knudsen numbers and similar to the two dimensional case.

To compare the speed up, we have considered again different resolutions, see Table 5.2, where the number of velocity grid points is again fixed. We observe for a resolution with $N = 30^3$ grid points a speed up of 127. For $N = 40^3$ grid points we obtain no further increase in speed up due to memory limitations.

In Table 5.3 we have presented the time spent on different tasks/kernels. We see that most of the time is used to approximate the spatial derivatives of the distribution function.

Moreover, in Fig. 5.4 we have plotted the comparison of computational time taken by CPU, OMP and GPU with different spatial resolutions for fixed velocity grid $N_v = 15$ at final time $t_{final} = 400 \times \Delta t$.

Finally, in Fig. 5.5 we have plotted the comparison of CPU, OMP and GPU with different velocity grids N_v while fixing the number of initial physical grid points to

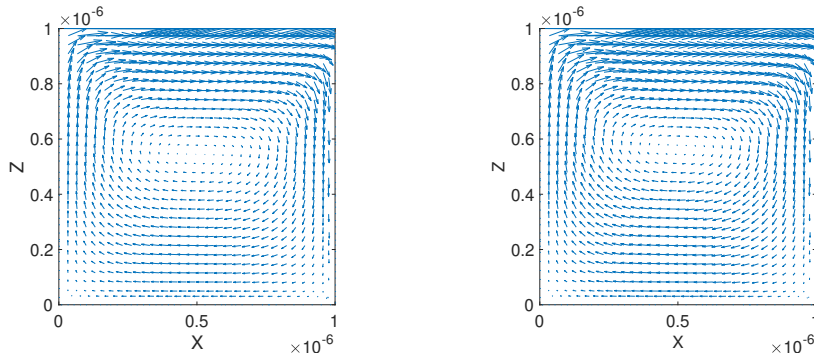


Fig. 5.3: Three dimensional velocity vectors in xz plane at half of the y -axis for Knudsen numbers and Reynolds numbers $Kn = 1.1, Re = 2.968 \times 10^{-4}$ (left) and $Kn = 0.11, Re = 2.968 \times 10^{-5}$ (right).

$N \times N_v^3$	Time (min)			Speedup		Memory
	CPU	OMP	GPU	CPU vs GPU	OMP vs GPU	
$20^3 \times 20^3$	1200	140	20	60	7	3.7GB
$30^3 \times 20^3$	4193	440	33	127	13	6.7GB
$40^3 \times 20^3$	10360	1040	93	115	11	14GB

Table 5.2: GPU Speedup for 3D Driven Cavity.

$N = 40^3$ at time $t_{final} = 400 \times \Delta t$.

6. Conclusion and Outlook. In this paper, we have presented an Arbitrary Lagrangian-Eulerian method for the simulation of the BGK equation with GPU parallelization. Besides the ALE approach, the method is based on first-order upwind approximations with the least squares method. Two-dimensional and three-dimensional test cases are performed. In the two-dimensional case, the GPU parallelization gives a speed of up to 300 times compared to a sequential CPU computation, while in a three-dimensional case, it is up to 120 times faster than the CPU computation. Compared to a parallel version of the CPU code we still obtain a speedup up to an order of magnitude.

In future work, the scheme will be extended to higher-order approximations using MPI and a multi-GPU optimized code. Furthermore, the case of gas-mixtures [17] and moving boundary problems, like coupling of the fluid flow to a rigid body motion, is considered in three-dimensional situations.

Acknowledgments. This work is supported by the DFG (German research foundation) under Grant No. KL 1105/30-1 and DAAD-DST India 2022-2024, Project-ID: 57622011 & DST/INT/DAAD/P-10/2022 and the European Union’s Framework Program for Research and Innovation HORIZON-MSCA-2021-DN-01 under the Marie Skłodowska-Curie Grant Agreement Project 101072546 – DATAHYKING.

REFERENCES

TASK/Kernel	Time Spent (%)
Spatial Derivative Approximation	80
Update Moment	1.63
Update Function	2.35
Interpolate Distribution Function on Boundary	10.69
Diffusive reflection Boundary Condition	4.59
Particle Organization	0.73

Table 5.3: Distribution time spent on each task per timestep on GPU.

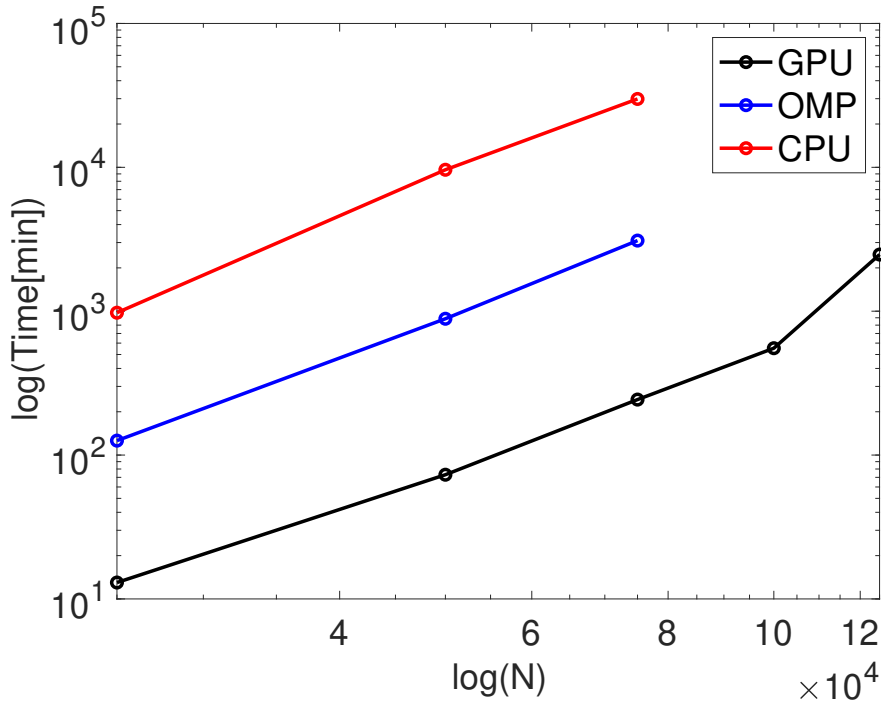


Fig. 5.4: Comparison of GPU, OMP and CPU time for 3D driven cavity problem for different numbers of initial spatial grid points for fixed velocity grids $N_v = 15$ at final time $t_{final} = 400 \times \Delta t$.

- [1] M. Andrea, L. Marco, T. Adriano, D. Mihir, R. Michele, A. Giorgio, B. Fabio, and S. Sauro. Thread-safe lattice boltzmann for high-performance computing on gpus. Journal of Computational Science, 74:102165, 2023.
- [2] T. Baier, S. Tiwari, S. Shrestha, A. Klar, and H. Hardt. Thermophoresis of Janus particles at large Knudsen numbers. Phys. Rev. Fluids, 3:094202, 2018.
- [3] G. Bird. Molecular Gas Dynamics and the Direct Simulation of Gas Flows. Clarendon Press, 1995.
- [4] S. Chapman and T. W. Cowling. The mathematical theory of non-uniform gases. Cambridge University Press, 1970.
- [5] C. K. Chu. Kinetic-theoretic description of the formation of a shock wave. Phys. Fluids, 8:12–21, 1965.

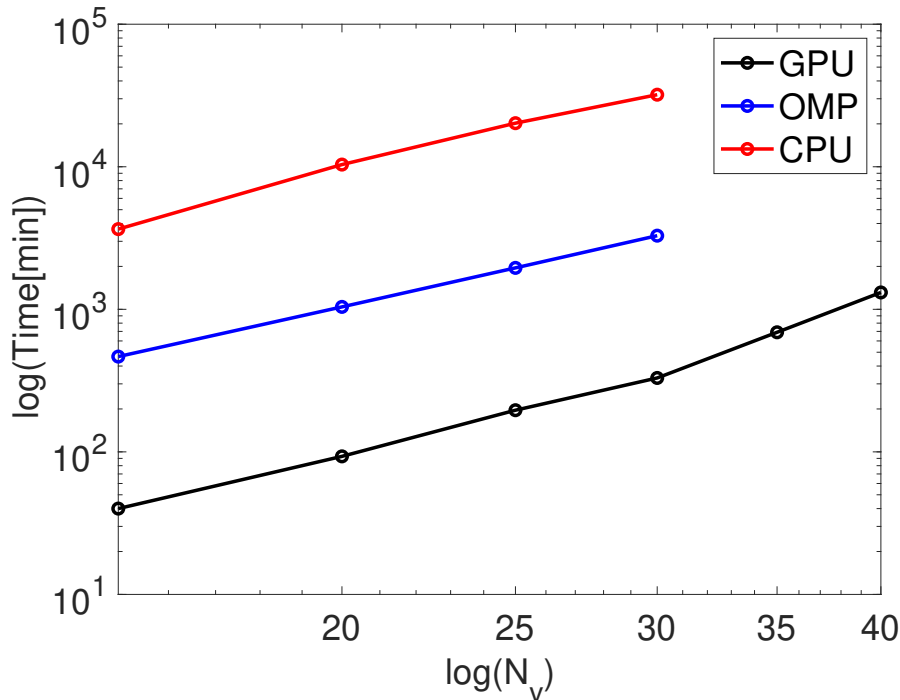


Fig. 5.5: Comparison of GPU, OMP and CPU time for 3D driven cavity problem for different numbers of velocity grid points for fixed number of initial spatial grid points $N = 40^3$ at final time $t_{final} = 400 \times \Delta t$.

- [6] F. E. De Vuyst, C. Labourdette, and C. Rey. Pu-accelerated real-time visualization and interaction for coupled fluid dynamics. *in: Proceedings CFM 2013*, 2013.
- [7] F. E. De Vuyst and F. Salvarani. Gpu-accelerated numerical simulations of the knudsen gas on time-dependent domain. *Comput. Phys. Commun.*, 184(3):532–536, 2013.
- [8] G. Dechristé and L. Mieussens. A Cartesian cut cell method for rarefied flow simulations around moving obstacles. *J. Comput. Phys.*, 314:465–488, 2016.
- [9] P. Degond, G. Dimarco, and L. Pareschi. The moment guided Monte Carlo method. *Int. J. Numer. Meth. Fluids*, 67:189–213, 2011.
- [10] G Dimarco, R. Loubere, and J. Narskl. Towards an ultra efficient kinetic scheme, part iii: High-performance computing. *Journal of Computational Physics*, 284:22–39, 2015.
- [11] Giacomo Dimarco and Lorenzo Pareschi. Numerical methods for kinetic equations. *Acta Numerica*, pages 369–520, 2014.
- [12] C. Drumm, S. Tiwari, J. Kuhnert, and H.-J. Bart. Finite pointset method for simulation of the liquid–liquid flow field in an extractor. *Computers & Chemical Engineering*, 32(12):2946–2957, 2008.
- [13] A Frezzotti and L. Ghiroldi. Solving model kinetic equations on gpus. *Comput. Fluids*, 50:136–146, 2011.
- [14] A Frezzotti and L. Ghiroldi. Solving the boltzmann equation on gpus. *Comput. Phys. Commun.*, 182:2445–2453, 2011.
- [15] A Frezzotti, L. Ghiroldi, and L. Gibelli. Direct solution of the boltzmann equation for a binary mixture on gpus. *in: Proceedings of the 27th International Symposium on Rarefied Gas Dynamics*, pages 884–889, 2011.
- [16] M. Groppi, G. Russo, and G. G. Stracquadanio. High order semi-Lagrangian methods for the BGK equation. *Commun. Math. Sci.*, 14(2):389–417, 2007.
- [17] M. Groppi, G. Russo, and G. Stracquadanio. Semi-Lagrangian approximation of BGK models

- for inert and reactive gas mixtures. P., Soares A. (eds) From Particle Systems to Partial Differential Equations. PSPDE 2016. Springer Proceedings in Mathematics & Statistics, 258, 2018.
- [18] Gaël Guennebaud, Benoît Jacob, et al. Eigen v3. <http://eigen.tuxfamily.org>, 2010.
- [19] G. Karniadakis, A. Beskok, and N. Aluru. Microflows and Nano- flows: Fundamentals and Simulations. Springer, New York, 2005.
- [20] J. Kuhnert. General smoothed particle hydrodynamics. PhD Thesis, University of Kaiserslautern, Germany, 1999.
- [21] J. E. Malkov and M. Ivanov. Parallelization of algorithms for solving the boltzmann equation for gpu-based computations. in: Proceedings of the 27th International Symposium on Rarefied Gas Dynamics, 182:946–951, 2011.
- [22] L. Peiyao, H. Changsheng, and G. Zhaoli. Gpu implementation of the discrete unified gas kinetic scheme for low-speed isothermal flows. Computer Physics Communications, 294:108908, 2024.
- [23] C. Praveen. A positive meshless method for hyperbolic equations. FM Report 2004-FM-16, Dept. of Aerospace Engg., IISc, India, 2004.
- [24] G. Russo and F. Filbet. Semi-Lagrangian schemes applied to moving boundary problems for the BGK model of rarefied gas dynamics. Kinetic and Related Models, Amer. Inst. Math. Sci., 2(1):231–250, 2009.
- [25] S. Shrestha, S. Tiwari, and A. Klar. Comparison of numerical simulations of the Boltzmann and the Navier-Stokes equations for a moving rigid circular body in a micro scaled cavity. Int. J. Adv. Eng. Sci. App. Math., 7(1-2):38–50, 2015.
- [26] S. Shrestha, S. Tiwari, A. Klar, and S. Hardt. Numerical simulation of a moving rigid body in a rarefied gas. J. Comput. Phys., 292:239–252, 2015.
- [27] T. Sonar. Difference operators from interpolating moving least squares and their deviation from optimality. ESAIM:M2AN, 39(5):883–908, 2005.
- [28] P. Suchde, J. Kuhnert, and S. Tiwari. On meshfree GFDM solvers for the incompressible Navier-Stokes equations. Computers and Fluids, 165:1–12, 2018.
- [29] T. Tadeusz and G. S. Roman. A new gpu implementation for lattice-boltzmann simulations on sparse geometries. Comput. Phys. Commun., 235:258–278, 2019.
- [30] S. Tiwari, A. Klar, and S. Hardt. A particle-particle hybrid method for kinetic and continuum equations. J. Comput. Phys., 228:7109–7124, 2009.
- [31] S. Tiwari, A. Klar, S. Hardt, and A. Donkov. Coupled solution of the Boltzmann and Navier–Stokes equations in gas–liquid two phase flow. Computers & Fluids, 71:283–296, 2013.
- [32] S. Tiwari, A. Klar, and G. Russo. A meshfree method for solving bgk model of rarefied gas dynamics. Int. J. Adv. Eng. Sci. Appl. Math., 11(3):187–197, 2019.
- [33] S. Tiwari, A. Klar, and G. Russo. Interaction of rigid body motion and rarefied gas dynamics based on the BGK model. Mathematics in Engineering, 2(2):203–229, 2020.
- [34] S. Tiwari, A. Klar, and G. Russo. A meshfree arbitrary lagrangian-eulerian method for the bgk model of the boltzmann equation with moving boundaries. Journal of Computational Physics, 458:111088, 2022.
- [35] T. Tsuji and K. Aoki. Moving boundary problems for a rarefied gas:spatially one dimensional case. J. Comput. Phys., 250:574–600, 2013.
- [36] T. Tsuji and K. Aoki. Gas motion in a microgap between a stationary plate and a plate oscillating in its normal direction. Microfluid Nanofluid, 16:1033–1045, 2014.
- [37] T. Xiong, G. Russo, and J.-M. Qiu. Conservative multi-dimensional semi-Lagrangian Finite Difference scheme: Stability and applications to the kinetic and fluid simulations. arXiv:1607.07409v1, 2016.
- [38] W. Yomsatieanku. High-Order Non-Oscillatory Schemes Using Meshfree Interpolating Moving Least Squares Reconstruction for Hyperbolic Conservation Laws. PhD Thesis, TU Carolo-Wilhelmina zu Braunschweig, Germany, 2010.
- [39] W. Yuhang, C. Guiyu, and P. Liang. Multiple-gpu accelerated high-order gas-kinetic scheme for direct numerical simulation of compressible turbulence. Journal of Computational Physics, 476:111899, 2023.